Odd-even mass differences from self-consistent mean field theory

G. F. Bertsch,[1] C. A. Bertulani,[2] W. Nazarewicz,[3,4,5] N. Schunck,[6] and M. V. Stoitsov[6]

[1]*Institute for Nuclear Theory and Department of Physics, University of Washington, Seattle, Washington, USA*
[2]*Department of Physics, Texas A&M University-Commerce, Commerce, Texas 75429, USA*
[3]*Department of Physics and Astronomy, University of Tennessee, Knoxville, Tennessee 37996, USA*
[4]*Oak Ridge National Laboratory, P.O. Box 2008, Oak Ridge, Tennessee 37831, USA*
[5]*Institute of Theoretical Physics, Warsaw University, ul.Hoża 69, PL-00681 Warsaw, Poland*
[6]*Institute of Nuclear Research and Nuclear Energy, Bulgarian Academy of Sciences, Sofia, Bulgaria*

We survey odd-even nuclear binding energy staggering using density functional theory with several treatments of the pairing interaction including the BCS, Hartree-Fock-Bogoliubov, and the Hartree-Fock-Bogoliubov with the Lipkin-Nogami approximation. We calculate the second difference of binding energies and compare the results with 443 measured neutron energy differences in isotope chains and 418 measured proton energy differences in isotone chains. The particle-hole part of the energy functional is taken as the SLy4 Skyrme parametrization, and the pairing part of the functional is based on a contact interaction with possible density dependence. An important feature of the data, reproduced by the theory, is the sharp gap quenching at magic numbers. With the strength of the interaction as a free parameter, the theory can reproduce the data to an rms accuracy of about 0.25 MeV. This is slightly better than a single-parameter phenomenological description but slightly poorer than the usual two-parameter phenomenological form c/A^{α}. The following conclusions can be made about the performance of common parametrization of the pairing interaction: (i) there is a weak preference for a surface-peaked neutron-neutron pairing, which might be attributable to many-body effects, (ii) a larger strength is required in the proton pairing channel than in the neutron pairing channel, and (iii) pairing strengths adjusted to the well-known spherical isotope chains are too weak to give a good overall fit to the mass differences.

I. INTRODUCTION

The theory of nuclear masses or binding energies has attracted renewed interest with the advent of computational resources sufficient to performed global calculations based on self-consistent mean field theory, also called density functional theory (DFT) [1–3]. A long-term goal is an improved reliability for a theory that avoids *ad hoc* phenomenological parametrizations. One particular aspect of the nuclear binding problem is the ubiquitous phenomenon of odd-even staggering (OES) of binding energy. Since the early days of BCS theory [4], OES has been largely attributed to BCS pairing, but there are in fact a number of mechanisms that can contribute [5–12]. In this work, we want to study the performance of BCS theory and its Hartree-Fock-Bogoliubov (HFB) extension to the global body of data, taking an energy density functional and pairing functionals that are in common use. In that way, we hope to provide a benchmark for assessing future improvements in the theory. Since we do not consider all mechanisms to generate the OES, our conclusions must be tentative.

There are many DFT surveys that treat individual isotope chains, e.g., Refs. [13,14], and the $Z = 50$ isotope chain is a favorite for the calculation of pairing properties. We shall see, however, that it can be quite misleading to draw general conclusions without examining the whole body of OES data. Also, in much of the literature, OES values were not obtained from differences of calculated binding energy but rather inferred from the average HFB gap parameters, as, e.g., in Ref. [15]. We also mention the global mass tables by the Brussels-Montreal Collaboration [16–18]. While this work achieves a good performance on binding energies, it deviates from the framework of DFT by adding phenomenological modifications to the theory. In particular, the pairing strength may depend on local densities, but it is hard to justify an explicit dependence on the number parity as is assumed in Ref. [18].

There are numerous measures of the OES in the literature, including 3-point, 4-point, and 5-point difference formulas [9,19–22]. In this work, we will use the 3-point formula $\Delta_o^{(3)}$ as advocated in Ref. [6] and also used in Refs. [10,15]. For odd neutron number N, it is defined by the binding energy difference

$$\Delta_o^{(3)}(N) = \tfrac{1}{2}\left[B(N+1) + B(N-1) - 2B(N)\right]. \quad (1)$$

In the following, we will call this quantity the "neutron OES." Our survey will cover the proton OES as well. One advantage of the $\Delta_o^{(3)}$ statistic is that it can be applied to more experimental data than the higher order ones. Another advantage is that it suppresses the smooth contributions from the mean field to the gap. The other 3-point indicator, $\Delta_e^{(3)}(N)$ with N even, is less interesting for our purposes, because it is more sensitive to single-particle energies.

This paper is organized as follows. Section II outlines the theoretical DFT framework employed in this work. In Sec. III the selection of experimental data used in the survey is discussed. The results for selected spherical and deformed isotopic/isotonic chains are presented in Sec. IV, while the global performance of our pairing models is analyzed in Sec. V. Finally, Sec. VI contains the main conclusions and perspectives.

II. METHODOLOGIES

We carry out two independent surveys with the same Skyrme functional SLy4 [23] in the particle-hole channel. The pairing functional uses the zero-range density-dependent δ interaction:

$$V(\mathbf{r}, \mathbf{r}') = V_0 \left(1 - \eta \frac{\rho(\mathbf{r})}{\rho_0}\right) \delta(\mathbf{r} - \mathbf{r}'). \qquad (2)$$

Here $V_0 < 0$ is the pairing strength, $\rho(\mathbf{r})$ is the isoscalar nucleonic density, and $\rho_0 = 0.16$ fm^{-3}. We have performed global calculations for $\eta = 0, 0.5$, and 1, called volume, mixed, and surface pairing, respectively. The volume pairing interaction acts primarily inside the nuclear volume, whereas the surface pairing generates pairing fields peaked around or outside the nuclear surface. As discussed in Refs. [24,25], different assumptions about the density dependence can result in notable differences of pairing fields in neutron-rich nuclei.

The two surveys were carried out assuming two different theoretical frameworks for the pairing channel: the BCS and the Hartree-Fock-Bogoliubov (HFB). The details are described in the two subsections below.

A. HF-BCS with EV8

The HF-BCS extension of the nuclear DFT can be defined very concisely. The ordinary variables in the theory, namely, the orbital wave functions ϕ_i expressed in some basis, are augmented by the BCS amplitudes v_i. Specifically, one defines the BCS v_i and u_i amplitudes for each orbital and calculates the ordinary DFT energy from its functional using the density matrix $\rho(\mathbf{r}, \mathbf{r}') = \sum_i v_i^2 \phi_i^*(\mathbf{r}) \phi_i(\mathbf{r}')$. To this is added the pairing energy functional, given by

$$E_{\text{pair}} = \sum_{i \neq j} V_{ij} u_i v_i u_j v_j + \sum_i V_{ii} v_i^2, \qquad (3)$$

where V_{ij} are the matrix elements of the pairing interaction.

We use the code EV8 [26] to carry out the HF+BCS computations. EV8 solves the HF+BCS equations for Skyrme-type functionals via a discretization of the individual wave functions on a three-dimensional Cartesian mesh and the imaginary time method. [In EV8, the pairing functional (3) is approximated as $\sum_{i,j} V_{ij} u_i v_i u_j v_j$.] The pairing interaction matrix elements are those of the density-dependent contact interaction (2). Contact interactions can only be used in truncated orbitals spaces; the calculations use the same truncation as is Ref. [27], namely, an energy window of 10 MeV around the Fermi level.

As we will see later, the OES only fluctuates about an average trend by $\sim$0.3 MeV, putting a high demand on the accuracy and the nucleus-to-nucleus consistency of the self-consistent mean field calculations. The usual iteration procedure in EV8 appears to be adequate to achieve accuracy at the 100 keV level in several hundred iterations at a fixed deformation.[1] Finding the minima irrespective of deformation

is less straightforward. We adopted the following protocol to determine them. We first build a table of DFT energies and orbital wave functions of the relevant even-even nuclei, using the minimum energy deformations from the table calculated in Ref. [27]. The relative energies of spherical and deformed configurations are quite sensitive to the pairing interaction, so when the spherical configuration in that table has an energy close to the deformed minimum, the spherical is also tested. When it comes out lower with the new pairing interaction, it replaces the old entry in the new table. Next, the table is refined in an iterative way, using only the deformation information about neighboring even-even nuclei. If two neighboring nuclei have substantially different deformations in the table, each configuration must be tested in both nuclei. If taking the lower energy configuration results in a change, the process is repeated on the neighbors of the replaced nucleus. This is continued until there are no further changes in the even-even DFT solutions.

Once the DFT table of even-even nucleus is finalized, the odd-A nuclei are calculated starting from the DFT solutions for the neighboring even-even nuclei. We perform the calculations using the so-called filling approximation for the odd particle [28,29]. The odd particle is assumed to occupy an orbital defined by its position in the list of orbitals ordered by single-particle energy. That orbital is blocked by setting $v^2 = u^2 = 0.5$ in the calculation of all ordinary densities and omitting the orbital in the summation in Eq. (3). During the self-consistency iterations, the blocked orbital evolves along with the others and thus may change character if the relative ordering of the levels changes. Note that the filling approximation gives equal occupation numbers to both time-reversed partners and therefore misses the effects of time-odd fields on the OES.

Our protocol to find the most favorable orbital to block was to examine the five orbitals around the Fermi level of the neighboring even-even system. We also tested configurations generated from the DFT solution for the even-even nucleus with one more nucleon than the target odd-A nucleus. Thus the total number of odd-A configurations tested was ten: five starting from the lighter even-even core and five starting from the heavier one.

Since the objective was to determine the level of accuracy that could be achieved, the calculations were carried out for the nuclei in the data set for a number of values of the pairing strength V_0. The results below are reported for a value V_0 close to that which minimizes the average residual in the $\Delta_o^{(3)}$ data sets, taking neutron and protons independently.

B. HFB with HFBTHO

The HFB calculations were carried out with the axial two-dimensional HFB solver HFBTHO [30] that has recently been improved by implementing the modified Broyden mixing [31] to accelerate the convergence rate.

The even-even nuclei are calculated first. An initial set of configurations is generated by performing constrained

---

[1] Here "accuracy" means with respect to the fully converged minimum of the numerically implemented energy functional. This numerical functional may contain approximations that give a larger error with respect to the mathematically defined functional. In the

case of EV8, the lattice representation of the kinetic operator results in an error of the order of 1 MeV in heavy nuclei, which varies very smoothly with A. Thus it largely cancels in the calculation of $\Delta_o^{(3)}$.

minimizations on a quadrupole deformation mesh. Typically, there are 20 calculations having deformations in the range $-0.5 < \beta < 0.5$ with a mesh spacing $\Delta\beta = 0.05$. Next, we turn off the constraint to find the local minima of the energy as a function of β. When there are multiple minima, we select up to three for further processing, taking no more than one of oblate and one of prolate deformation and also the spherical solution if it is a local minimum. The final step is to perform unconstrained minimizations on the selected configurations. The iterative minimization is carried out until the maximum change of the HFB matrix elements falls below 0.0001 MeV. However, in one case, the iteration converges to a limit cycle with energies oscillating by 0.004 MeV. Since this is well below the accuracy needed here, we accepted the (lowest) calculated energy.

The minimization for odd N or Z is started from the candidate configurations produced at the second stage of the even-even calculations. As in the BCS, the odd nucleus is treated in the filling approximation, by blocking one of the orbitals. Here one has to specify which orbitals to block to generate the odd-nucleon configurations. The blocking candidates are determined by examining the HFB quasiparticle spectrum of the smaller neighboring even-even nucleus. Tested are all one-quasiparticle configurations with quasiparticle energies below the energy cutoff $E_{1qp,cut}$, which is not smaller than 2 MeV for heavy nuclei and not bigger than 8 MeV for very light systems. For most nuclei, we take $E_{1qp,cut} = 25/\sqrt{A}$ MeV. As in the last step for even-even nuclei, unconstrained calculations are performed for all candidate configurations to find the absolute minimum energy.

In the second variant of HFB calculations (HFB+LN), we performed an approximate particle number projection (before variation) using the Lipkin-Nogami (LN) method [32,33]. The practical implementation of the LN treatment follows Ref. [34], where the method was compared with the full particle number projection.

In HFB and HFB+LN calculations, we employed the orbital space extending to 20 major harmonic oscillator shells. For the pairing interaction, there is no lower energy orbital cutoff; and for the upper equivalent energy cutoff ,we adopted the commonly used value of 60 MeV [35]. The calculations were first performed with a standard pairing strength V_0^{std} adjusted to the average pairing gap in ^{120}Sn according to the procedure of Ref. [36]. The values obtained are $V_0^{std} = -258.2$ and -284.57 for the HFB and the HFB+LN calculations. However, following our first survey, we found these strengths to be too small to make a good global fit to OES. We then increased the pairing strength by a factor of 1.2 and recalculated the mass table from scratch. Both sets of tables are available through the UNEDF SciDAC Collaboration [37]. Our fit to the global systematics is then made using a linear fit of the data sets of the two mass tables:

$$M(x) = xM\left(V_0^{std}\right) + (1 - x)M\left(1.2V_0^{std}\right). \quad (4)$$

The effective pairing strength obtained in this way is given by

$$V_0^{eff} = (1.2 - 0.2x)V_0^{std}. \quad (5)$$

The values of x and the derived pairing strengths are reported in Table I.

TABLE I. Effective strengths for the pairing interactions derived in the present study by means of Eq. (4). Units of V_0 are MeV fm^3. Also the values of the fit parameter x are given in parentheses.

Theory	Density dependence	$V_0^{nn}(x)$	$V_0^{pp}(x)$
BCS	Volume	465.0	490.0
	Mixed	700.0	755.0
	Surface	1300.0	1462.0
HFB	Mixed	318.1(0.41)	352.0(−0.18)
HFB+LN	Mixed	300.5(0.18)	332.6(−0.44)

C. Other methodological aspects

In setting up the calculational protocols for the survey, we of course scrutinized cases in which the residuals between theory and experiment were large. The residuals are very sensitive to numerical inaccuracies, and their detailed analysis often brought to our attention problems with calculated numbers due to, e.g., incorrectly assigned configurations or the lack of convergence in self-consistent iterations. We could then refine the protocols by making a broader screen or demanding higher precision to produce more accurate tables. From this standpoint, we found $\Delta_o^{(3)}$ to be a very useful indicator. Also, the fact that the theory is variational is a tremendous help: any change in protocol that gives lower energies is necessarily an improvement.

Apart from the numerics, it should be noted that the pairing gap is a very strong function of the pairing strength. For example, for the HFB calculations, we found that increasing the pairing strength by 20% from the value fitted to ^{120}Sn caused the average neutron pairing gap to increase by a factor of 2.3. This sensitivity is not surprising. A typical nucleus in our set has some deformation and does not have a large single-particle degeneracy at the Fermi level. This implies that its BCS condensate is weak. Under these conditions, the BCS gap increases very quickly from a zero value at some finite strength of the interaction. In fact, we find that roughly 20–30% of the calculated OESs contain a nucleus whose BCS or HFB condensate has collapsed. Even in infinite systems having no single-particle gap at the Fermi energy, the condensate Δ grows exponentially with interaction strength in the well-known BCS formula.

An exact implementation of HFB requires the breaking of the time-reversal symmetry in the intrinsic frame of an odd-A nucleus. The resulting time-odd mean fields contribute to the binding energy of the odd-A system; hence, the OES $\Delta_o^{(3)}$ depends on whether these time-odd terms are included or not [7,8,11,12,38]. In general, time-odd mean fields are poorly known, and their effects differ from model to model. For instance, in the Skyrme DFT calculations of Ref. [38], the time-odd polarizations systematically shift the hole states down and particle states up in energy, while a different result has been obtained in the relativistic mean field approach [7,8]. For the purpose of illustration, Fig. 1 shows the OES values calculated in the HFB for isotonic chains including the effects of time-odd fields. A detailed analysis of resulting polarizations will be published elsewhere [40]. It appears that the contribution is less that 100 keV in heavy elements such as the rare earths and
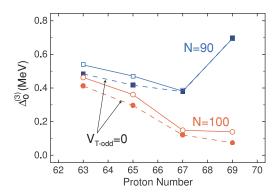
FIG. 1. (Color online) Impact of time-odd terms on the proton OES $\Delta_o^{(3)}$ in the $N = 90$ and 100 isotonic chains calculated in the HFB theory with SLy4 functional and mixed pairing. Solid lines connect the values of proton OESs including time-odd fields; dashed lines show the OES values omitting the time-odd fields. Calculations were performed with the code HFODD of Ref. [39] in a deformed harmonic oscillator (HO) basis containing 680 deformed HO states.

actinides, but larger values have been found with other models, e.g., Refs. [8,12], and in light nuclei. In any case, the density functional has not been fitted to time-odd properties, so no quantitative evaluation of their effect is possible. In this work, we employ the filling approximation, neglecting all time-odd interactions.

III. EXPERIMENTAL DATA BASE

The data base for our survey derives from the 2003 atomic mass evaluation [41]. The accuracy requirements for our purposes is of the order of 100 keV, so we only use the masses whose evaluated experimental errors are less than 200 keV. This gives 908 mass triplets for the neutron OESs and 864 for protons. However, we made additional cuts to remove nuclei for which some physics is obviously missing from our BCS or HFB theory. First of all, in odd-odd nuclei there is an additional neutron-proton pairing effect. Its origin is not completely clear [42], but it is obviously beyond the scope of the pairing theory we use here. We therefore do not include binding energy triplets containing odd-odd nuclei. Another phenomenon in nuclear binding that affects the OES is the so-called Wigner energy, an increased binding at $N = Z$. This might also be a neutron-proton pairing effect (see, e.g., Refs. [43,44]). We therefore eliminate triplets that contain $N = Z$ nuclei. More generally, mean field approximations become doubtful when the number of particles is small. Some restriction of light nuclei is imposed by a cut on particle numbers, requiring that the neutron and proton numbers be greater than 8, corresponding to nuclei heavier than ^{16}O. Finally, we only include nuclei with $N > Z$. There are only a few OESs on the proton-rich side satisfying our other criteria, and keeping a fixed sign of the isospin will permit us to make some qualitative statement about the isospin dependence of the interaction. With all these cuts, 443 triplets are left for the neutron OES and 418 for the proton in our final data set.

The sets of neutron and proton $\Delta_o^{(3)}$ are plotted as a function of neutron and proton number in the top panels of Fig. 2. Lines connect the OES values for the same number of nucleons of

the opposite kind. It is common to plot OES as a function of A, but plotting it with respect to nucleons of the same kind makes clearer the origin of fluctuations. Probably the largest cause of fluctuation is the variation in single-particle level densities and the character of the level at the Fermi energy. This obviously depends strongly on the number of nucleons of the same kind, and this motivates the choice of abscissa variable. The single-particle level densities may also change with the different numbers of nucleons of the other kind, particular if the additional nucleons causes a large change in deformation. Such effects should be visible in the variation of OES at fixed value of the abscissa. To emphasize the like-nucleon fluctuations, we also show as solid circles the average with respect to nucleons of the opposite kind.

One can see that the shell effects are large, and there are large fluctuations on the scale of major shell spacings. For the neutron values of $\Delta_o^{(3)}$, there are strong dips in the Z-averaged values at $N = 15, 29, 51, 83,$ and 125, i.e., in the vicinity of shell closures. We call this phenomenon "gap quenching." Obviously, the OES is reduced when one of the three nuclei is at a magic number where the gap in single-particle energies is large. We will examine the effect in more detail below, in presenting the theoretical OES. In Table II, we show the extreme OES cases—either the largest or the smallest in our experimental data sets.

Another observation that can be made about the neutron OES is that the variations with respect to Z are particularly large in the regions $N = 50$ and 95–110. For the protons, the regions of strongest N dependence are $N = 35$ and 60–70. We will see that this is associated, at least in part, with changing deformations.

The averages and variances for neutron and proton OES $\Delta_o^{(3)}$ in the data set are 1.04 ± 0.31 and 0.96 ± 0.27 MeV, respectively. The lower average for the protons can be largely attributed to the Coulomb interaction: in the liquid-drop formula, the term $a_c Z^2/A^{1/3}$ gives an average value of 0.11 MeV for the proton $\Delta_o^{(3)}$ in the data set. There is some overall dependence of the OES on mass number A, which may be seen by visual inspection of Fig. 2. For more discussion of the global mass dependence of the OES, we refer the reader to Refs. [6,15,22]. The smooth A dependence seems rather weak compared to the local nucleus-to-nucleus fluctuations caused by shell effects, but parametrizing it in some way can give improved fits. For example, the phenomenological parametrization [19,45]

$$\tilde{\Delta} = \frac{c}{A^\alpha}, \qquad (6)$$

with $c = 4.66\,(4.31)$ MeV and $\alpha = 0.31$ gives an rms residual of 0.25 MeV on the neutron (proton) data set. The global

TABLE II. Nuclei from the data base adopted for our survey with the largest and smallest experimental values of $\Delta_o^{(3)}$ (in MeV).

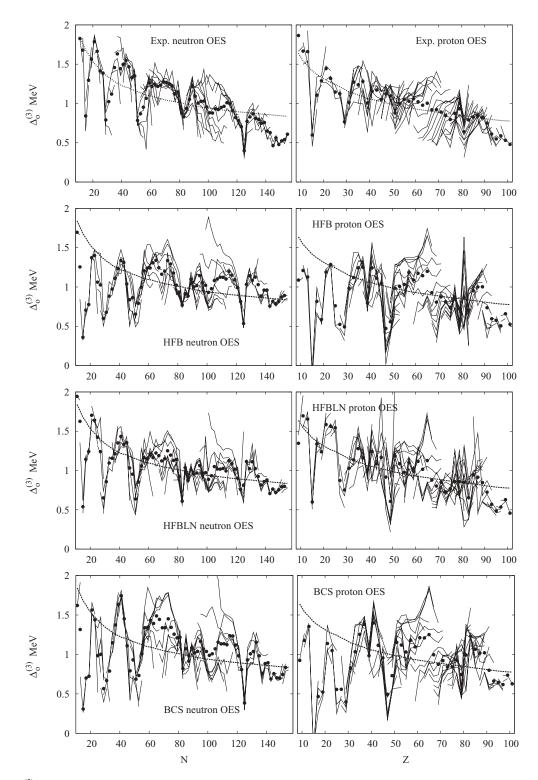|	Largest		Smallest	
	(N, Z)	$\Delta_o^{(3)}$	(N, Z)	$\Delta_o^{(3)}$
Neutrons	(21, 16)	1.87	(125, 82)	0.32
Protons	(12, 9)	2.07	(126, 81)	0.31

FIG. 2. OES $\Delta_o^{(3)}$ as a function of nucleon number for experiment, HFB, HFB+LN, and BCS treatments. Solid circles show values obtained by averaging over nucleon number of the opposite isospin to that of the OES. The calculation used the SLy4 Skyrme energy functional and a pairing interaction with the mixed density dependence.

trends given by Eq. (6) are shown as the dashed lines in Fig. 2. For the sake of the plot, we averaged over nucleon number of the opposite kind just as was done to produce experimental averages.

An important question about the global systematics is whether there is an isospin dependence of the pairing interaction. It is clear from Fig. 2 that there can be strong interaction between the pairing of one kind on the numbers
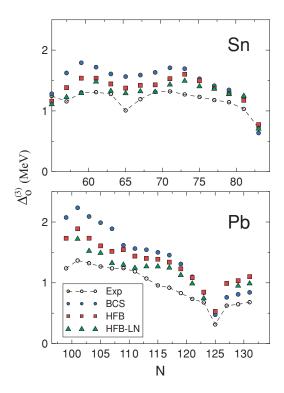
FIG. 3. (Color online) Calculated (HF+BCS, HFB, and HFB+LN) and experimental values of $\Delta_o^{(3)}$ for neutrons in the Sn and Pb semimagic isotopic chains. In all calculations, the pairing interaction was taken in the mixed pairing form ($\eta = 0.5$) with strength V_0 [or x in Eq. (4)] adjusted to global systematics.

of the other kind, but as mentioned it could be due to other effects such as shape changes. The isospin dependence has been examined in Ref. [22], but no significant effect has been found (see also Refs. [46–48] for more discussion of isovector trends). On the other hand, a recent study [49] of the OES of nuclear masses for isotopic chains between the proton shell closures at $Z = 50$ and $Z = 82$, including nuclei with extreme isospins, has claimed a significant isospin dependence of pairing. We will discuss in more detail the possible evidence for an isovector dependence of the interaction in Sec. V C.

IV. RESULTS: LOCAL COMPARISONS

We begin our comparison between theory and experiment with two spherical semimagic isotope chains, Sn and Pb. The results of the calculations are shown in Fig. 3.
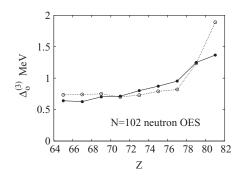

FIG. 5. Experimental (filled circles) and HFB (open circles) neutron OES for $N = 102$ as a function of Z. The chain starts in the well-deformed lanthanides and ends next to the singly magic ^{184}Pb.

For all three treatments of pairing, the trends of the predicted OESs are consistent with the data, concerning both global and local variations. In particular, theory reproduces the flatness in the Sn isotopes up to the quenched gap at $N = 83$, and the downsloping trend from the light Pb isotopes up to the quenched gap at ^{207}Pb. In the Sn isotope chain, there is a small dip at $N = 65$, which might be attributed to a neutron subshell closure at $N = 64$. In any case, the theories all predict a shallow local minimum. When confronted with experiment, HFB appears to do slightly better than HF+BCS. As mentioned earlier, the strength of the pairing interaction was fit to the overall systematics, giving a somewhat too high average OES in both spherical chains.

The performance of the theories for long isotonic and isotopic chains that include deformed nuclei is illustrated in Figs. 4 and 5. Figure 4 shows the neutron values of OES in the Dy isotopes ($Z = 66$) and proton OES values in the $N = 98$ isotones. As for semimagic nuclei, the agreement with experiment is good, particularly for well-deformed nuclei where the mean field changes smoothly with particle number. The effect of changing deformation is illustrated by the region from $A \sim 160$ to ~ 190, which starts deformed and becomes spherical as Z is increased from 66 to 82. The neutron values of OES for $N = 102$ covering this transition region are shown in Fig. 5 as a function of Z. The squares show the experimental OES values, which increase from about 0.6–0.8 MeV for the lower Z nuclei and goes up to ~ 1.3 MeV for the singly magic $Z = 82$ isotope. The circles show the corresponding calculated HFB values of OES. The trend is very similar, but the theoretical rise to $Z = 82$ is sharper and higher than is seen experimentally. Very likely, the increase in single-particle level
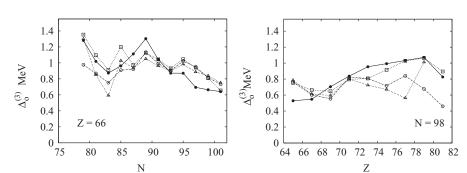

FIG. 4. Calculated and experimental values of $\Delta_o^{(3)}$ for neutrons ($Z = 66$) and protons ($N = 98$) in rare earth nuclei, including strongly deformed systems. Filled circles: experiment; squares: BCS; open circles HFB; triangles: HFB+LN.

density going from deformed to spherical nuclei is responsible for the increasing trend in the OES.

The fact that our calculations overestimate OES values in spherical nuclei may be partly attributed to the particle number fluctuations. The pairing gap exponentially depends on the inverse of the single-particle level density at the Fermi level, which is large in spherical open-shell nuclei because of the $2j + 1$ degeneracy (the limit of pairing rotation). In deformed systems, the level density is reduced because of the Jahn-Teller effect [50,51], and this gives rise to the overall pairing reduction; hence, a transition occurs toward the transitional pairing regime, in which the particle number fluctuations are more important. Since the original pairing strength V_0^{std} was adjusted to the global data set containing far more nonspherical nuclei than semimagic systems, the resulting deformation bias results in too strong pairing correlations predicted for spherical nuclei, as seen in Fig. 3. This can be partly cured by considering particle number fluctuations. Indeed, as seen in Figs. 3 and 4, the LN procedure slightly improves the agreement with experiment for spherical nuclei while still reproducing data for deformed chains.

V. RESULTS: GLOBAL

A. Overview and shell effects

Figure 2 shows the distributions of neutron and proton OES values for our three theoretical treatments: HFB, HFB+LN, and BCS. To make the overall trends with respect to shell filling more apparent, we also show the values of the OES obtained by averaging over nucleons of the opposite isospin. Qualitatively, the three methodologies give rather similar results. In all cases, the trends of the predicted gaps are consistent with the data. The strong neutron gap quenching seen in the experimental OES at the numbers $N = 83$ and $N = 125$ is reproduced in all three theoretical treatments. The gap quenching is obviously dependent on the presence of shell closures, but the fact that it does not invariably occur on both sides of the magic numbers indicates that particular orbital properties must play a role. Since the HFB calculations were performed in an axially symmetric basis, we can examine the quantum numbers of the blocked orbital.

In Table III, we show the quasiparticle orbital characteristics for odd nuclei exhibiting quenched gaps. The large quenching at $N = 125$ can be understood as a spherical shell effect associated with the $p_{1/2}$ shell at the Fermi level. A $j = 1/2$ shell will have reduced pairing for two reasons. First, there is no degeneracy within the shell to correlate pairs, so all of the pairing has to come from off-diagonal interactions to other shells. Second, these couplings are reduced because the spatial overlap of high-l and low-l orbitals is poor. Similar considerations apply to $N = 15$ and $Z = 81$, where the relevant spherical shell is $s_{1/2}$.

While the location of the gap quenching is well reproduced by theory, the magnitude of the effect is often exaggerated. Most notably, all the experimental OES values are positive, the theoretical ones at $(N, Z) = (20, 15)$ even have a negative sign.

TABLE III. Characteristics of nuclei with quenched gaps in the HFB calculations. The listed nucleus is the one with the smallest OES value at the given gap. The calculated deformation β is given in the third column. The last columns give the quasiparticle quantum numbers angular momentum and parity J^π for spherical nuclei and azimuthal angular momentum K and parity $K\pi$ for deformed nuclei.

	Nucleus	β	j^π or K^π
N gap:			
15	^{25}Ne	0.00	$1/2^+$
29	^{52}Ti	0.08	$1/2^-$
47–51	^{87}Kr	−0.09	$5/2^+$
83	^{147}Gd	−0.03	$7/2^-$
125	^{125}Pb	0.00	$1/2^-$
Z gap:			
15	^{39}P	0.21	$1/2^+$
29	^{61}Cu	0.10	$3/2^-$
47–49	^{111}Ag	−0.22	$1/2^+$
69	^{173}Tm	0.33	$7/2^-$
81	^{203}Tl	0.01	$1/2^+$

Comparing the different treatments of pairing, we see fluctuations at the same positions in BCS and HFB+LN as in the HFB. However, the amplitudes of the fluctuations seem somewhat larger in the BCS treatment but somewhat smaller in HFB+LN. It is not clear why the BCS should emphasize the fluctuations, but the fact that they are damped in HFB+LN is not surprising. In both BCS and HFB the static pairing sometimes collapses in a significant fraction of nuclei, as mentioned earlier. The pairing never collapses in the HFB+LN treatment, so the OES should be smoother as one passes into a region of weak pairing.

Large variations with proton number are found around $N \sim 70$ and in the region $N = 100$. As mentioned earlier, the latter region is a transition region between spherical and deformed ground states, and that will affect the OES. The HFB theory has a spike as well as quenched-gap behavior at $Z = 81$ in the proton gap. The origin of the spike appears to be the coexistence of spherical and deformed configurations in light isotopes of $Z = 81$ and 82 nuclides. At the phase transition point, there can be a large static polarization contribution to the OES.

To see where theory performs best and where important physics is missing, we show in Fig. 6 the isospin-averaged residuals for our HFB model. As expected, the best agreement is obtained for well-deformed rare earths and actinides whose properties vary smoothly with particle number. The largest deviations are seen around shell closures and in the regions of shape coexistence ($A \sim 90$ for neutrons and $A = 110$ and 190 for protons) where dynamic shape fluctuations are known to strongly impact masses [27,52].

To analyze more quantitatively the improvement in accuracy for deformed nuclei, we examined the rms residuals for the neutron OES values, separating the data into bins by the calculated values of the deformation β. Figure 7 shows the averaged HFB residuals. As expected, the residuals gradually decrease with deformation. The transitional/coexisting nuclei
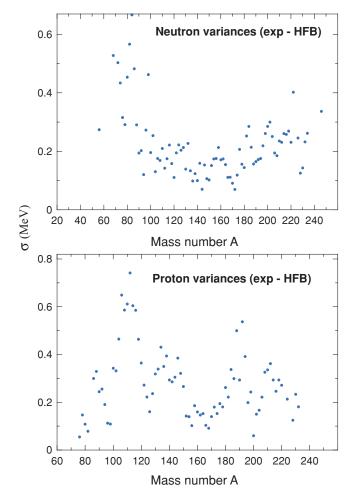
FIG. 6. (Color online) Neutron and proton average variances σ between HFB and experimental $\Delta_o^{(3)}$ as a function of A. At each A, the variance σ was obtained by averaging the residuals over all isobars available.

FIG. 7. Neutron average variances σ between HFB and experimental $\Delta_o^{(3)}$ as a function of the calculated quadrupole deformation β_2. The deformation range $-0.2 \leqslant \beta_2 \leqslant 0.4$ was divided into bins with $\Delta\beta_2 = 0.1$, and for each bin the variance σ was obtained by averaging the residuals over all nuclei available.

below another mechanism that could simulate the observed trend in A, namely, an isospin dependence of the effective pairing interaction.

with weakly oblate shapes show the largest deviations from the data.

The fluctuations in OES are obviously suppressed when one averages over nucleons of the opposite isospin. With that averaging, the comparison between theory and experiment looks much better. Figure 8 shows the theory vs experiment comparison for the HFB methodology. Besides seeing the shell effects discussed above, one also sees more clearly how the theory performs with respect to the A dependence of the pairing. The theoretical proton OES has an overall A dependence that seems to accord well with the experimental trend. For the neutron OES, however, the theory is flatter than the experimental trend.

We carried out the survey with different assumptions about the density dependence of the pairing interaction to observe any sensitivity of the A dependence to that characteristic. The results of the averaged neutron OES for volume and surface pairing are shown in Fig. 9. The effect is very small, except for the light nuclei. In view of the other possible contributions to the staggering, we do not believe that one can reliably extract the density dependence of the effective pairing interaction strength from the observed A dependence. We discuss
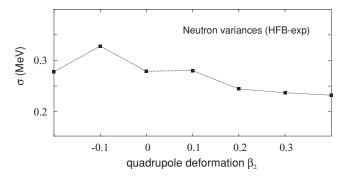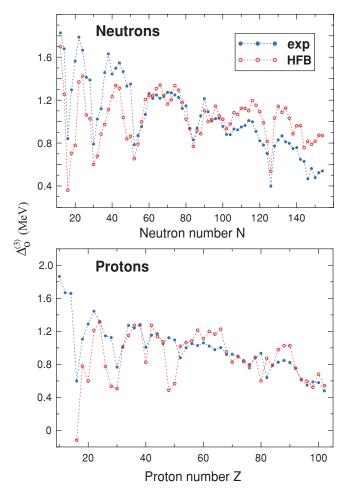

FIG. 8. (Color online) Comparison between calculated (HFB with mixed pairing) and experimental $\Delta_o^{(3)}$ values, plotting Z-averaged values for neutrons and N-averaged values for protons.
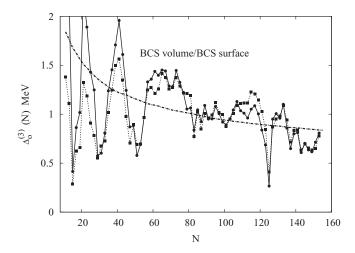
FIG. 9. Averaged BCS neutron OES values with the volume (squares connected by dotted line) and surface (circles connected by solid line) pairing interactions of Eq. (2). The dot-dashed curve is the phenomenological fit to the data using the functional form (6).

B. Performance statistics

In Table IV, we report the rms residuals for the OES in the various treatments, fitting the strength of the pairing interaction separately for neutrons and protons. In the case of our HFB and HFB+LN models, we carried out separate optimizations for neutrons and protons with respect to the x parameter in Eq. (4). The effective pairing strength obtained in this way is given by Eq. (5). A more proper procedure would be to make a two-dimensional optimization based on recalculated HFB mass tables assuming different strengths of proton and neutron pairing. Our experience with HF+BCS model, however, is that the neutron pairing strength does not significantly affect the proton $\Delta_o^{(3)}$ and vice versa, at the level of changes considered in this work. Therefore, for the purpose of a global survey, a simplified treatment has been adopted.

From Table IV we see that all three treatments of the pairing can achieve the performance of zeroth order description as a constant (or phenomenological) gap, but only the Lipkin-Nogami, shown on the next-to-last line, does significantly

TABLE IV. Root-mean-square residuals of $\Delta_o^{(3)}$ obtained in various models. All energies are in MeV. The last column shows the ratio of proton and neutron effective pairing strengths obtained through the optimization procedure. The mass predictions of the HFB-14 model [17] were taken from Ref. [53].

Theory	Pairing	Residual neutrons	Residual protons	$V_0^{\text{eff}}(p)/V_0^{\text{eff}}(n)$
Constant		0.31	0.27	
c/A^α		0.24	0.22	
HF+BCS	Volume	0.31	0.38	1.05
HF+BCS	Mixed	0.30	0.36	1.08
HF+BCS	Surface	0.27	0.35	1.12
HFB	Mixed	0.27	0.33	1.11
HFB+LN	Mixed	0.23	0.28	1.11
HFB-14		0.46	0.44	1.10

better. In the HFB+LN, pairing correlations are always present. This is particularly important for odd-A nuclei, where the standard blocking procedure often gives rise to the unphysical pairing collapse, artificially affecting the OES and producing an exaggerated fluctuation. However, one should be cautious in using the HFB+LN. While for open-shell systems using it gives a good agreement with those of the HFB with the full particle number projection before variation, the method is inaccurate for closed-shell systems [34]. Consequently, it is safest to use HFB+LN only away from the magic numbers. In addition, the numerical procedure to find the solution lacks stability when there is a large gap at the Fermi level. Nevertheless, we obtained converged solutions for 440 of the 443 neutron triplets and 411 of the 418 proton triplets with our HFB+LN implementation. The numbers in Table IV are for those data sets. If we restrict the data set further to omit the magic numbers 28, 50, 82, and 126, the rms residual of the neutron OES is hardly affected, changing from 0.23 to 0.22.

One of the basic questions about nuclear pairing is the role of induced interactions in the effective pairing interaction [5,54–57]. Indirect information about this can in principle be obtained by exhibiting the density dependence and the isospin dependence of the effective interaction. It is therefore of interest to examine interactions including a density dependence to see the sensitivity. The rms residual for the neutron OES with volume, mixed, and surface pairing in HF+BCS theory are shown in Table IV. There is a slight favoring of the surface interaction, but we deem that the difference in the residuals (10%) is too slight to be significant. The weak sensitivity to the density dependence confirms the results of other studies [10,58].

C. Isospin dependence

A possible isospin dependence of the effective pairing strength has been much discussed in the literature [22,46–48, 59,60]. The nuclear interaction may be assumed to conserve isospin at a fundamental level, but the coupling to core excitations can be different for neutrons and protons when the core has a neutron excess. Another isospin-dependent contribution to pairing comes from the Coulomb interaction. Indeed, inclusion of the Coulomb has been found to substantially suppress the pairing interaction energy [61] and the pairing gaps [56]. In the last column of the Table IV, we report the ratio of neutron and proton interaction strengths extracted from our fits to $\Delta_o^{(3)}$. The effective proton strength, needed to reproduce experimental $\Delta_o^{(3)}$, is larger than the neutron strength. If the Coulomb were included explicitly, we would expect that the needed nuclear interaction would be even larger for the protons. Since the underlying strong interaction is isoscalar to a good approximation, we believe that our inferred isospin effect must arise from induced three-body interactions involving the neutron excess. We note in passing that a number of mass table fits by the Goriely group arrive at pairing strengths larger for protons than neutrons. An example is the HFB-14 model [17], shown in the last line of Table IV. However, since different interactions are used for even and odd nuclei in HFB-14, the results are not directly comparable.

TABLE V. Average $\Delta_o^{(3)}$ (in MeV) calculated in HFB+LN sorted by neutron excess. See text for details.

	Data set	Low isospin	High isospin	Difference
Neutrons	Exp	1.13	0.94	−0.19
	HFB+LN	1.05	1.02	−0.03
Protons	Exp	1.05	0.88	−0.17
	HFB+LN	0.99	0.93	−0.06

As another way to test the data for an isospin-dependent pairing interaction, we separate the nuclei into two subsets according to neutron excess and compare the average residual OESs. To define the subsets, we first divide the nuclei into five A bins. For each bin, we make a cut at some value of $I = (N - Z)/A$ to have roughly equal numbers for the two sets, which we designate "low isospin" and "high isospin." In that way, the effect of any A dependence in the OES will be reduced. The binning for proton and neutron values of $\Delta_o^{(3)}$ has to be done separate to get balanced sets. The average values of OES for the two sets are reported in Table V.

The empirical OES is lower for higher neutron excesses for both protons and neutrons. The calculated $\Delta_o^{(3)}$ for neutrons are nearly equal, while the calculated $\Delta_o^{(3)}$ for protons do show a difference but much smaller than observed. For both cases, the differences would require weakening the pairing interaction for nuclei with larger neutron excesses. An isospin dependence would have the opposite sign for proton and neutron gaps.

As a final plausibility check on whether the different strengths could be attributable to some isoscalar three-body interaction, we computed the OES values for nuclei on the opposite side of the $N = Z$ line (recall that our fitted data set is restricted to $N > Z$). This comprises five neutron OESs and six proton OESs, excluding as before cases involving $N = Z$ nuclei. Taking the pairing strengths from our global fit, we find that the calculated average neutron OES is too low (by 0.7 MeV), while the calculated average proton OES is too high (by 0.24 MeV). This is precisely the expected direction of the error if the difference in the effective strengths depends on the sign of $N - Z$, as would be required by an overall isoscalar energy functional.[2]

Thus, the main evidence for an isospin dependence in the present theory is the need for different strengths for the overall fits to neutron and proton data sets. This result supports the recent attempts [59,60] to directly parametrize the pairing functional in terms of isovector densities.

VI. PERSPECTIVE

The present study demonstrates that the current state of the art in the nuclear DFT permits calculation of OES values to an accuracy of the order of 0.25 MeV rms. This is not a trivial outcome in two respects. First, the binding energies involved range up to nearly four orders of magnitude larger, so there is a high demand on computational precision in performing the

DFT. Second, the pairing gap is a highly sensitive function of the mean field properties such as level density, and so the theory needs to have an accurate treatment of the single-particle properties. In this work, we have only considered the SLy4 functional, which has known deficiencies. Clearly, further exploration of DFT functionals is warranted, perhaps including ones having different (isoscalar and isovector) effective masses.

We found no large differences between the BCS and HFB treatments. This is not unexpected; it is only near the drip lines that the HFB with its better treatment of spacial variations of the anomalous density is needed. On the other hand, we believe that the improvement we found for the HFB+LN treatment is significant, showing that a number-conserving treatment of the pairing correlations is needed. Many of the nuclei, particularly the odd ones, are on the edge of collapse of BCS pairing, and for these a number-conserving treatment is essential to calculate the pairing correlation energy. Unfortunately, the LN treatment of number violation is not reliable near closed shells. We would therefore advocate in the future using other treatments of number violation, perhaps HFB with variation-after-projection [34], or mapping onto an exactly soluble pairing Hamiltonian [62].

The global data on OES shows a weak A dependence that is certainly not reproduced with a pairing interaction that is density independent or has only a mild dependence on density. In the calculations with the BCS theory, the sensitivity to density dependence was explored, and it was found that there were only small changes in the overall performance. It should also be noted that the mean field contributions to the OES are highly dependent on A. Thus, firm conclusions about the origin of the A dependence must await surveys based on theory that avoids the filling approximation.

A very interesting question related to density dependence is whether there is an isospin dependence of the strength of the effective pairing interaction. The question cannot be addressed with confidence by examining individual isotope or isotone chains, because the other species of nucleon can affect the effective pairing Hamiltonian, particularly the single-particle spectrum. However, from the global survey, we find what seems to be a robust result, that the effective pairing strength for protons OES is about 10% larger than for neutron OES. The calculation does not take into account the Coulomb interaction in the pairing channel, but naively that would be expected to decrease the effect strength, not increase it. The other possible explanation of the difference is an induced isospin dependence.

It is perhaps disappointing that the overall performance of the theory is only slightly better than the naive one-parameter phenomenology attributing the staggering to a constant BCS gap. The two-parameter phenomenological function c/A^α does slightly better than the theory overall. But that form has no justification, and the shell effects that are faithfully reproduced by the theory are missing. So we conclude that the rms residuals between theory and experiment do not tell the whole story. In any case, the promising possibility to surpass the performance of the present phenomenology is to continue the DFT studies with better functionals, including mean field contributions and number-conserving treatments of pairing.

---

[2]We are indebted to A. Bulgac for calling our attention to this point.

[1] M. Bender, P.-H. Heenen, and P.-G. Reinhard, Rev. Mod. Phys. **75**, 121 (2003).

[2] M. V. Stoitsov, J. Dobaczewski, W. Nazarewicz, and P. Borycki, Int. J. Mass Spectrom. **251**, 243 (2006).

[3] G. F. Bertsch, D. J. Dean, and W. Nazarewicz, SciDAC Rev., Issue 6, 42 (2007).

[4] A. Bohr, B. R. Mottelson, and D. Pines, Phys. Rev. **110**, 936 (1958).

[5] D. M. Brink and R. A. Broglia, *Nuclear Superfluidity: Pairing in Finite Systems* (Cambridge University, Cambridge, England, 2005).

[6] W. Satuła, J. Dobaczewski, and W. Nazarewicz, Phys. Rev. Lett. **81**, 3599 (1998).

[7] K. Rutz, M. Bender, J. A. Maruhn, P.-G. Reinhard, and W. Greiner, Nucl. Phys. **A634**, 67 (1998).

[8] K. Rutz, M. Bender, P.-G. Reinhard, and J. Maruhn, Phys. Lett. **B468**, 1 (1999).

[9] M. Bender, K. Rutz, P.-G. Reinhard, and J. A. Maruhn, Eur. Phys. J. A **8**, 59 (2000).

[10] J. Dobaczewski, P. Magierski, W. Nazarewicz, W. Satuła, and Z. Szymaski, Phys. Rev. C **63**, 024308 (2001).

[11] T. Duguet, P. Bonche, P.-H. Heenen, and J. Meyer, Phys. Rev. C **65**, 014310 (2001).

[12] T. Duguet, P. Bonche, P.-H. Heenen, and J. Meyer, Phys. Rev. C **65**, 014311 (2001).

[13] J. Dobaczewski, W. Nazarewicz, and M. V. Stoitsov, in *Proceedings of the NATO Advanced Research Workshop, The Nuclear Many-Body Problem 2001, Brijuni, Croatia, 2–5 June 2001,* edited by W. Nazarewicz and D. Vretenar (Kluwer, Dordrecht, 2002), p. 181.

[14] Y. Yu and A. Bulgac, Phys. Rev. Lett. **90**, 022501 (2003).

[15] S. Hilaire, J. Berger, M. Girod, W. Satuła, and P. Schuck, Phys. Lett. B **531**, 61 (2002).

[16] S. Goriely, M. Samyn, P. H. Heenen, J. M. Pearson, and F. Tondeur, Phys. Rev. C **66**, 024326 (2002).

[17] S. Goriely, M. Samyn, and J. M. Pearson, Phys. Rev. C **75**, 064312 (2007).

[18] N. Chamel, S. Goriely, and J. M. Pearson, Nucl. Phys. **A812**, 72 (2008).

[19] A. Bohr and B. R. Mottelson, *Nuclear Structure* (Benjamin, New York, 1969), Vol. I.

[20] A. S. Jensen, P. G. Hansen, and B. Jonson, Nucl. Phys. **A431**, 393 (1984).

[21] D. G. Madland and R. Nix, Nucl. Phys. **A476**, 1 (1988).

[22] P. Möller and R. Nix, Nucl. Phys. **A536**, 20 (1992).

[23] E. Chabanat, P. Bonche, P. Haensel, J. Meyer, and R. Schaeffer, Nucl. Phys. **A635**, 231 (1998); **A643**, 441(E) (1998).

[24] J. Dobaczewski, W. Nazarewicz, and P.-G. Reinhard, Nucl. Phys. **A693**, 361 (2001).

[25] J. Dobaczewski, W. Nazarewicz, and M. V. Stoitsov, Eur. Phys. J. A **15**, 21 (2002).

[26] P. Bonche, H. Flocard, and P. H. Heenen, Comput. Phys. Commun. **171**, 49 (2005).

[27] M. Bender, G. F. Bertsch, and P.-H. Heenen, Phys. Rev. C **73**, 034322 (2006).

[28] S. Perez-Martin and L. M. Robledo Phys. Rev. C **78**, 014304 (2008).

[29] G. Bertsch, J. Dobaczewski, W. Nazarewicz, and J. Pei, arXiv:0808.1874.

[30] M. V. Stoitsov, J. Dobaczewski, W. Nazarewicz, and P. Ring, Comput. Phys. Commun. **167**, 43 (2005).

[31] A. Baran, A. Bulgac, Michael McNeil Forbes, G. Hagen, W. Nazarewicz, N. Schunck, and M. V. Stoitsov, Phys. Rev. C **78**, 014318 (2008).

[32] H. J. Lipkin, Ann. Phys. (NY) **9**, 272 (1960).

[33] Y. Nogami, Phys. Rev. **134**, B313 (1964).

[34] M. V. Stoitsov, J. Dobaczewski, R. Kirchner, W. Nazarewicz, and J. Terasaki, Phys. Rev. C **76**, 014308 (2007).

[35] J. Dobaczewski, M. Stoitsov, and W. Nazarewicz, AIP Conf. Proc. **726**, 51 (2004).

[36] J. Dobaczewski, W. Nazarewicz, and T. Werner, Phys. Scr. **T56**, 15 (1995).

[37] http://unedf.org/content/tools.php or massexplorer.org.

[38] M. Zalewski, J. Dobaczewski, W. Satuła, and T. R. Werner, Phys. Rev. C **77**, 024316 (2008).

[39] J. Dobaczewski and P. Olbratowski, Comput. Phys. Commun. **158**, 158 (2004); **167**, 214 (2005).

[40] N. Schunck, J. Dobaczewski, J. D. McDonnell, W. Nazarewicz, and M. V. Stoitsov (in preparation).

[41] G. Audi, A. H. Wapstra, and C. Thibault, Nucl. Phys. **A729**, 337 (2003).

[42] W. A. Friedman and G. F. Bertsch, Phys. Rev. C **76**, 057301 (2007).

[43] W. Satuła, D. J. Dean, J. Gary, S. Mizutori, and W. Nazarewicz, Phys. Lett. **B407**, 103 (1997).

[44] W. Satuła and R. Wyss, Phys. Rev. Lett. **86**, 4488 (2001); **87**, 052504 (2001).

[45] H. Olofsson, S. Åberg, and P. Leboeuf, Phys. Rev. Lett. **100**, 037005 (2008).

[46] P. Vogel, B. Jonson, and P. G. Hansen, Phys. Lett. **B139**, 227 (1984).

[47] A. S. Jensen and A. Miranda, Nucl. Phys. **A449**, 331 (1986).

[48] V. E. Starodubsky and M. V. Zverev, Phys. Lett. **B276**, 269 (1992).

[49] Yu. A. Litvinov, T. J. Bürvenich, H. Geissel, Yu. N. Novikov, Z. Patyk, C. Scheidenberger, F. Attallah, G. Audi, K. Beckert, F. Bosch, M. Falch, B. Franzke, M. Hausmann, Th. Kerscher, O. Klepper, H.-J. Kluge, C. Kozhuharov, K. E. G. Löbner, D. G. Madland, J. A. Maruhn, G. Münzenberg, F. Nolden, T. Radon, M. Steck, S. Typel, and H. Wollnik, Phys. Rev. Lett. **95**, 042501 (2005).

[50] P.-G. Reinhard and E. W. Otten, Nucl. Phys. **A420**, 173 (1984).

[51] W. Nazarewicz, Nucl. Phys. **A574**, 27c (1994).

[52] M. Bender, G. F. Bertsch, and P.-H. Heenen, Phys. Rev. Lett. **94**, 102503 (2005).

[53] http://www-astro.ulb.ac.be/Html/hfb14.html.

[54] P. Donati, G. Gori, F. Barranco, R. A. Broglia, and E. Vigezzi, J. Phys. G **31**, 295 (2005).

[55] T. Duguet and T. Lesinski, Eur. Phys. J. ST **156**, 207 (2008).

[56] T. Lesinski, T. Duguet, K. Bennaceur, and J. Meyer, arXiv:0809.2895.

[57] R. A. Broglia, F. Barranco, P. F. Bortignon, G. Colò, and E. Vigezzi, Phys. Scr. T **125**, 94 (2006).

[58] N. Sandulescu, P. Schuck, and X. Viñas, Phys. Rev. C **71**, 054303 (2005).

[59] J. Margueron, H. Sagawa, and K. Hagino, Phys. Rev. C **76**, 064316 (2007).

[60] M. Yamagami and Y. R. Shimizu, Phys. Rev. C **77**, 064319 (2008).

[61] M. Anguiano, J. L. Egido, and L. M. Robledo, Nucl. Phys. **A683**, 227 (2001).

[62] R. A. Senkov, G. F. Bertsch, B. A. Brown, Y. L. Luo, and V. G. Zelevinsky, Phys. Rev. C **78**, 044304 (2008).